Applied Catalysis B: Environmental 84 (2008) 667–677

Contents lists available at ScienceDirect

Applied Catalysis B: Environmental

journal homepage: www.elsevier.com/locate/apcatb

Hydrodechlorination of *para*-substituted chlorobenzenes over a ruthenium/carbon catalyst

Tetsuya Yoneda [a,*], Toshio Takido [b], Kenji Konuma [a]

[a] Department of Liberal Arts and Science, College of Science and Technology, Nihon University, Narashinodai 7-24-1, Funabashi, Chiba 274-8501, Japan
[b] Department of Materials and Applied Chemistry, College of Science and Technology, Nihon University, Kanda-surugadai 1-8-14, Chiyoda, Tokyo 101-8308, Japan

ARTICLE INFO

Article history:
Received 29 September 2007
Received in revised form 24 May 2008
Accepted 26 May 2008
Available online 5 June 2008

Keywords:
Hydrodechlorination
Para-substituted chlorobenzenes
Ru/C catalyst
DFT
Adsorption energy

ABSTRACT

The hydrodechlorination (HDC) of chlorobenzene (abbreviated as CLB) and seven types of *para*-substituted chlorobenzenes (*para*-amino, -methoxy, -methyl, -chloro, -trifluoromethyl, -acetyl and -cyano: abbreviated as CLAN, CLAS, CLTN, DCLB, CLTF, CLAP and CLBN, respectively) were performed over 5%-ruthenium/carbon (Ru/C) under a hydrogen pressure of 0.5–1.5 MPa at 523 K.

In the HDC of these model compounds, except for CLAP and CLBN, reductive cleavage between the carbon and chlorine atoms took place and dechlorinated compounds were produced preferentially. In the reaction of CLAP and CLBN, on the other hand, hydrogenation and/or hydrogenolysis of the substituent coincided with the HDC and a wide variety of products was observed accompanying the HDC product.

For the chlorobenzenes of the simple HDC, the HDC reaction rate constants decreased in the orders of CLAN $\gg$ CLB $\approx$ CLTN $\approx$ CLAS and CLB $>$ DCLB $\gg$ CLTF, respectively.

In the reaction of the chlorobenzenes of the electron-donating substituent, the reaction constant ($\ln k/k_0$) has no relevance to the Hammett substituent constant (σ_p^0). In the case of the chlorobenzenes possessing the electron-withdrawing substituent, on the other hand, it was indicated that the electron-withdrawing substituent suppressed the HDC reactivity of chlorobenzenes, although no proportional relationship was observed between the reaction rate constant and the Hammett substituent constant.

To explore the factors affecting the HDC reactivity, quantum calculation according to the DFT method (B3LYP/LANL2DZ) was applied to the "chlorobenzenes-Ru_{10}" complex. As a result of the calculation, chlorobenzenes were adsorbed through a chlorine atom on the edge atom of the Ru_{10} cluster. The magnitude of the adsorption energy, moreover, decreased in the order of CLAN $>$ CLAS $\approx$ CLB $\approx$ CLTN and CLB $>$ DCLB $>$ CLTF, respectively. These orders of adsorption energy are similar to that of the HDC reaction rate constant. It was concluded that adsorption energy is a useful parameter for the reactivity index of the HDC.

1. Introduction

Since organic chlorinated compounds such as PCBs and HCH are harmful not only in rubbish and waste but are also carcinogenic substances, appropriate chemical disposal is required to protect human health and preserve the environment. Chlorinated compounds can be degraded by combustion [1,2], pyrolysis [3], electrolysis [4,5], ultra-violet irradiation [6], ultrasonic reaction [7,8], biological disposal [7,9], microwave reaction [10] and catalytic hydrogenolysis [11–28]. Of these methods, catalytic hydrodechlorination (HDC) is simple, safe, and effective [11], because hydrogen chloride is easily separated from the process as a by-product, and refined hydrocarbons can be recycled.

For the HDC reaction, many reports deal with the reaction mechanism [12,13], catalytic activity [14,15] and the preparation or modification of the catalyst [16–18]. However, few studies focus on the HDC reactivity of chloro-aromatics [19–23]. For instance, in the gas phase reaction of chlorobenzene and its derivatives with electron-donated substituents over the Ni/SiO_2 catalyst, Keane [19] suggested that the higher dechlorination rates were indicative of an electrophilic mechanism.

In the liquid phase reaction of the HDC of the substituted chlorobenzenes over Pd/C catalyst [20], we found that both the electron-releasing groups and the electron-withdrawing groups accelerate the HDC, and that linear relationships between the reaction rate constant ($\ln(k/k_0)$) and the Hammett constant (σ_p^0) were observed in each group. In contrast, Wu et al. [22] reported

* Corresponding author. Tel.: +81 47 469 5310; fax: +81 47 469 5310.
E-mail address: yoneda@chem.ge.cst.nihon-u.ac.jp (T. Yoneda).

0926-3373/$ – see front matter © 2008 Elsevier B.V. All rights reserved.
doi:10.1016/j.apcatb.2008.05.024

that electron-donating and electron-withdrawing groups suppressed the reaction rate constants in the liquid phase reaction over Ni/C, Ni/γ-Al_2O_3, Ni/SiO_2 and Raney Ni. Recently, we showed that the effect of the electron-withdrawing substituent over the platinum/carbon (Pt/C) catalyst suppresses the reaction rate of the substituted chlorobenzenes [23].

However, for these distinct kinetic studies, consensus on the electronic factors affecting the HDC reactivity of chlorobenzenes has not been reached beyond the differences in the catalytic elements and other reaction conditions. We are currently searching for a certain unity of HDC activity about the platinum group catalysts according to periodic metal elements or groups. To elucidate the electronic factors affecting these HDC, hence, we need to study other metal catalysts such as Ru, Rh, Co, Ni and so forth, comprehensively.

In the present study, chlorobenzene (abbreviated as CLB) and seven types of *para*-substituted derivatives: amino-, methoxy-, methyl-, chloro-, trifluoromethyl-, acetyl- and cyano-chlorobenzene (abbreviated as CLAN, CLAS, CLTN, DCLB, CLTF, CLAP and CLBN, respectively) were hydrogenolyzed over a ruthenium-carbon (Ru/C) catalyst under hydrogen pressure of 1 MPa at 523 K in a batch reactor. Since the substituent effect in the HDC of chlorinated organic compounds has not been reported for the ruthenium catalyst [15,24–27], the reaction rate was measured and the relevancy of the rate constants to Hammett's substituted constants was checked. Furthermore, in order to explain the HDC reactivity from the standpoint of the adsorption energy, the quantum calculation was performed according to the density functional theory method.

2. Experimental

2.1. Materials

Chlorobenzene, the *para*-isomers of chlorotoluene (CLTN), dichlorobenzene (DCLB), and chlorobenzonitrile (CLBN) were obtained from Kanto Kagaku Co. Ltd. The *para*-isomers of chloroaniline (CLAN), chloroanisole (CLAS), chloroacetophenone (CLAP) and trifluoromethyl-chlorobenzene (CLTF) were purchased from Tokyo Kasei Kogyo Co. Ltd. Solvents of 1,3,5-trimethylbenzene and hexadecane were produced by Kanto Kagaku Co. Ltd. These substrates and solvent, except for hexadecane, were purified according to a conventional method before use. The carbon-supported 5%-ruthenium catalyst (Ru/C), supplied by Sigma–Aldrich Co., was used without purification and the particle size of the catalyst was less than 45 μm (>330 mesh).

2.2. Apparatus and reaction procedure

The HDC reaction was carried out in a test tube (Pyrex glass, i.d. 28 mm × height 130 mm, volume: approx. 77 ml) that was placed into a magnetically stirred autoclave (Sakashita Seisakusho, SUS316, volume: approx. 108 ml) in a batch system. Both the sampling tube (i.d. 0.25 mm × length 600 mm) and the liquid introducing vessel (SUS304, volume: 50 ml) were equipped with an autoclave lid. In order to maintain effective agitation of the reactants, three rectangular turbulence boards (length 60 mm × width 4 mm × thickness 1.5 mm, glass) were fusion-bonded onto the inner wall of the test tube with three points. This experimental apparatus is described in a previous paper [20].

The Ru/C catalyst (0.01 g) was placed into the test tube in the autoclave. After purging the air of the autoclave with hydrogen gas, the catalyst was reduced at a hydrogen flow rate of 100 ml/min under 0.5 MPa at 573 K for 1 h and a liquid introducing vessel was placed on the inlet part of the autoclave. Hexadecane (35 ml), as the main solvent, was deposited into the vessel and then purged by hydrogen gas. At the termination of this reduction, the residual hydrogen gas in the autoclave was rapidly released, and the hexadecane in the vessel was introduced to the test tube with 0.3 MPa of hydrogen pressure. As soon as the pressure in the reactor was adjusted to 0.5 MPa at 558 K, both the solvent and catalyst in the test tube were stirred at 1200 rpm. When the temperature of the reactor was maintained at 523 K, the reactant solution (concentrations: 25×10^{-3} to 100×10^{-3} mol/l) of 1,3,5-trimethyl-benzene (5 ml) was added from the liquid introducing vessel, using hydrogen gas of 0.8 MPa and following a pressure adjustment to 1.0 MPa.

In the course of the reaction, the hydrogen pressure and temperature were kept at 1.0 ± 0.05 MPa and 523 ± 1 K, respectively. Concerning the chlorobenzenes except for DCLB, the range of the starting Cl (mol)/Ru (g) ratios was ca. 2–8 mol/g. For DCLB, possessing two chlorine atoms in the molecule, the range was estimated at ca. 4–16 mol/g. The HDC conversion was stopped within 15 mol%, in order to avoid the effect of products on the reaction rate. In the course of the reaction, reaction products were periodically extracted via the pressure-resistant valve.

2.3. Catalyst characterization

For a Ru/C catalyst, the metal content was measured by an Inductively Coupled Plasma Atomic Emission Spectrometer (ICP-AES, Shimadzu Co., CPS-8100) from the diluted dissolution, following fusion by sodium peroxide and dry ashing.

The BET surface area and pore size distribution measurement were determined using the BELSORP-mini (BEL Japan Inc.) apparatus. After outgasing at 393 K, a nitrogen adsorption isotherm was employed to determine the total surface area using the standard multiple point BET method at 77 K. Mesopore and micropore volumes were measured using BJH, MP and *t*-plot methods, which are based on a carbon standard curve endorsed by BEL Japan.

The metal surface area, dispersion and average metal particle size were obtained from gas-chemisorption analyses of both carbon monoxide (CO) and hydrogen (H_2) (BEL-METAL-3SP, BEL Japan Inc.). The samples (0.03 g) were loaded into a U-shaped Pyrex glass cell (i.d. 3.5 mm, volume 5 ml) and reduced in hydrogen at 573 K for 60 min, as same as in the experimental pre-reduction of the catalyst. Following the reduction, the samples were swept with 50 ml/min inert gases dried for 90 min (helium gas in CO chemisorption, argon gas in H_2 chemisorption), cooled to 323 K and subjected to each chemisorption using a pulse (10 %-CO/He or 10 %-H_2/Ar, ca. 0.13–0.14 ml at a time) titration procedure in He flow (50 ml/min).

Temperature-programmed experiments on both the decomposition of the functional group on the carbon surface (TPD) and reduction (H_2-TPR) on the Ru/C catalyst were carried out in an apparatus consisting of a differential flow reactor coupled to a mass spectrometer (TPD-1-ATw, BEL Japan Inc.). In both cases, approximately 0.1 g of sample was heated at 20 K/min up to 1073 K. During the TPD experiments, helium was passed thorough the reactor at a flow rate of 60 ml/min. For H_2-TPR experiments, a mixture of 5%-H_2 in helium was used with a flow rate of 60 ml/min, while the gas analyses were carried out by mass spectrometry.

Powder X-ray diffractograms (XRD) were recorded with a D8-Focus (Bruker AXS K.K.) using nickel filtered Cu Kα radiation. The samples were mounted in a low background sample holder and scanned at a rate of 0.02° per step over the $5^\circ \leq 2\theta \leq 70^\circ$ range at a scan speed of 0.06° min^{-1} at 298 K. The diffractograms were compared with the JCPDS-PDF references (No. 6-0663 [29], 26–1079, and 40–1290: Ru, C, and RuO_2, respectively) for identification purposes.

2.4. Product analysis

The products were analyzed by gas chromatography (Shimadzu Co., GC-14A or 14BPTF) using wide bore capillary columns (Varian, CP-sil 13CB or CP-wax 52CB, i.d. 0.53 mm × length 100 m or 0.53 mm × 60 m, respectively) and helium as a carrier gas (flow rate: 20 ml/min), equipped with a flame ionization detector. These analyses quantitatively utilized an internal standard method with toluene or *meta*-xylene. Products were identified by gas chromatography–mass spectroscopy (Shimadzu Co., GC-MS5050QA) fitting a narrow bore capillary column (J&W Scientific, DB-1, i.d. 0.25 mm × length 60 m).

The initial reaction rates were determined by plotting the concentration of the dechlorinated product versus the reaction time. The trinomial expressions ($r = at^3 + bt^2 + ct$) were applied to these plotted data, where the coefficient of the first term (c) at 0 min ($t = 0$) was used for the reaction rate $(dr/dt)_{t=0}$.

2.5. Quantum calculation

The quantum calculation was performed according to the spin-restricted density functional theory (DFT) method [30] that is implemented in the software package GAUSSIAN03 (Gaussian Inc., Rev. C. 01). Geometry optimization of the chlorobenzenes and the chlorobenzenes-ruthenium complexes were practiced by the B3LYP/LANL2DZ system. The B3LYP method, which consists of Becke three plus LYP parameters [31,32], includes hybrid functionals, being a mixture of Hartree-Fock exchange with DFT exchange-correlation terms. The LANL2DZ basis set exchanges the inner core orbitals for the Los Alamos Effective Core Potentials [33]. The convergence criteria with default values as follows: the maximum force, the RMS force, the maximum displacement and the RMS displacement were 0.00045, 0.0003, 0.0018 and 0.0012, respectively.

Ru-clusters were constructed of the lattice constants of Swanson et al. ($a = 0.27058$ nm, $c = 0.42819$ nm) in the point group of $D_{6h}^4 - P6_3/mmc$ [29]. Bond lengths, angles and dihedral angles among ruthenium atomics were fixed in all optimized computations, while the chlorobenzenes of the "chlorobenzenes-Ru_{10}" cluster were fully optimized in all cases.

3. Results and discussion

3.1. Catalyst characterization

3.1.1. Textural properties

The physicochemical properties of the Ru/C catalyst are given in Table 1 and the metal surface area analyses were calculated from two individual pulse gas-chemisorption results assuming a stoichiometric atom ratio (CO:Ru = 1:1, or H:Ru = 1:1, respectively). The several textural values were obtained using the spherical metal model on carbon-support, according to a ruthenium density of 12.41 g/cm^3, atomic weight of 101.07 and atomic surface area of 0.0613 nm^2/atom. In order to clarify the difference in the HDC activities of Ru/C and Pt/C catalysts, the data for the later catalyst that was used in the previous study [23] is also described in Table 1.

As shown in Table 1, the CO chemisorption volume of the Ru/C (6.2 ml/g) is considerably large when compared with the H_2 chemisorption (0.88 ml/g), so that the metal particle size of CO chemisorption was approximately three times the size of the H_2 chemisorption result. In the case of Pt/C, it was also observed that the CO chemisorption volume is higher than the H_2 chemisorption volume. Indeed, both techniques have been utilized in many researches on heterogeneous catalysis, as well as a transmission electron microscope (TEM). However, when these techniques were applied to the same or similar catalysts (e.g. Ni/C, Ni/Al_2O_3, Ni/SiO_2), incoherent results were observed in several reports [22,34], depending on the support, metal element, and catalyst preparation. At present, it is inferred that the large CO adsorption volume is probably overestimated by the formation of certain types of ruthenium complexes such as $Ru(CO)_n$, where the subscription number is more than 1 ($n > 1$). In this paper, the difference in the activity between Ru/C and Pt/C is discussed from the data of H_2 chemisorption.

Table 1
Textural characteristic of the Ru/C and Pt/C catalyst

N_2-gas sorption	Ru/C		Pt/C	
Metal loading (w/w%)	4.5		4.9[a]	
BET surface area (m^2/g)	836		966[a]	
Mesopore volume (cm^3/g)	0.52[b], 0.53[c]		0.35[a,b], 0.36[a,c]	
Micropore volume (cm^3/g)	0.31[d], 0.29 [e]		0.36[a,d], 0.45[a,e]	
Pore diameter (nm)[d]	0.75		0.97[a]	
Pulse gas-chemisorption	**CO method**	**H_2 method**	**CO method**	**H_2 method**
Adsorption volume (ml/g)[f]	6.2	0.88	0.74[a]	0.21
Metal surface area (m^2/g)	10	2.9	3.1[a]	0.9
Average metal particle size (nm)	2.1	7.5	3.7[a]	15
Dispersion (%)	62	18	13[a]	7.5

[a] These values for the Pt/C catalyst were measured in a previous study [23].
[b] BJH method associated with absorption.
[c] BJH method associated with desorption.
[d] MP method.
[e] *t*-Plot method.
[f] STP, 0.101 MPa and 273 K.

As for the HDC of chlorobenzene (CLB: 100×10^{-3} mol/l) for 30 min and at 523 K, the turnover frequency (TOF) over Ru/C (16.5 min^{-1}) on the basis of the H_2 chemisorption was fairly superior to that over Pt/C (5.7 min^{-1}), where the turnover frequency is the mol ratio of substrate (mol)/active metal atom (mol) per unit time, and the active metal atom is the surface atom here. This result means that the HDC reactivity over the Ru/C catalyst is more active than that over the Pt/C catalyst [23].

3.1.2. Temperature-programmed examination

In order to understand the surface oxygen groups on carbon-support in detail, temperature-programmed decomposition (TPD) was used to characterize the Ru/C catalyst. The CO_2- and CO-releasing profiles are shown in Fig. 1, where the axis of the ordinate expresses μmol/g. It can be seen that CO_2 is evolved mainly between 350 and 800 K (peak top is 559 K), while the CO evolution

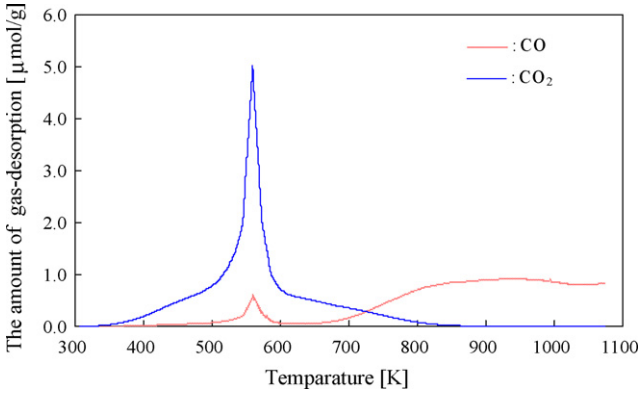

Fig. 1. Carbon monoxide (CO) and carbon dioxide (CO_2) quantifications in the temperature-programmed decomposition (TPD) for surface oxygen groups on carbon-support of Ru/C catalyst.

Table 2
TPD and TPR quantifications of the Ru/C catalyst

Gas	Peak temperature (K)	Evolved amount (μmol/g)	Total amount of evolution (μmol/g)
TPD			
CO_2	559	853.0	853.0
CO	559	77.3	
	944	751.4	908.6
	1072	80.0	
Gas	**Peak temperature (K)**	**Consumed amount (μmol/g)**	**Total amount of consumption (μmol/g)**
H_2-TPR			
H_2	369	118.0	1843.5
	752	1725.5	
H_2O	389	−[239.1][a]	−[649.7][a]
	752	−[649.7][a]	

[a] Expression by ionic intensity (count × $1/10^4$) of H_2O, due to the lower reliability of quantity by μmol/g.

takes place from 500 to 600 K and above 650 K (peak tops are 559, 944 and 1072 K). In addition, the total amounts of CO_2 and CO evolution were 853 and 909 μmol/g, respectively (see Table 2).

The evolution of CO_2 and CO gases is considered attributable to the decomposition of the different surface oxygen groups present on the carbon surface in a TPD experiment. Furthermore, it has been reported that relatively stronger acid groups, like carboxylic acid and/or anhydride spices, are decomposed into CO_2 at a lower temperature range, whereas the relatively weaker acid groups (i.e. lactone, carbonyl, phenol groups) lead to CO evolution at a higher temperature range [35]. Based on these conceptions, it may be supposed that equal amounts of the functional groups of the stronger and weaker acid are present on the carbon-support.

To gain more information on the catalyst surface, the catalyst was also subject to an H_2-TPR experiment. The hydrogen consumption profile is shown in Fig. 2. Initially, there was a lower reductive peak at 369 K. Huang et al. thoroughly investigated the characterization of the surface composition of platinum and ruthenium nano-alloys dispersed on active carbon using XRD and H_2-TPR [36] and assigned the peak at $T = 370$ K to the reduction of the amorphous RuO_2 prepared by calcinations at 300, 370, and/or 470 K,

$$RuO_2\ (\text{amorphous}) + 2H_2 \rightarrow Ru + 2H_2O \quad (1)$$

while the peak at $T = 450$ K of the RuO_2 produced by the calcinations at a high temperature over 570 K was assigned to the reduction of the crystalline RuO_2. Stuchinskaya et al. also reported that the reduction from bulk RuO_2 to Ru^0 occurred quantitatively at about 370 K in the H_2-TPR profile [37]. Furthermore, Yin et al. studied the hydrogen consumptions of the ruthenium catalyst on several supports at temperatures of around 430–510 K, indicating the significance of the intensity of interaction between RuO_2 and the support [38].

Under these circumstances, the lower peak of the hydrogen consumption at 369 K might be caused by the reaction of Eq. (1) on the Ru/C surface. The fact that the water evolution peak was confirmed at the neighboring temperature (389 K) leads us to the above consideration. The higher peak of the TPD profile in Fig. 2 at $T = 752$ K may be assigned to the decomposition of several carbon surface groups as a considerable amount of water was detected within the same temperature range. These assignments, however, must be investigated in more detail.

3.1.3. X-ray diffraction analysis

In order to observe the catalyst surface in detail, X-ray diffraction (XRD) analysis was applied to both the Ru/C catalyst before and after the reduction for 5 h at 573 K, as seen in Fig. 3. The high peak at 26.6° derived from the carbon-support was observed. However, none of the intensive peaks for the crystal (that are characterized at 38.4°, 42.2°, 44.0°, 58.3°, 69.4°, 78.4°, 84.7°and 86.0°) were detected by XRD analysis [39]. The weak intensity peaks for the RuO_2 of the rutile type (that are characterized at 28.4°, 35.1°, 40.0°, and 54.2° corresponding to the (1 1 0), (1 0 1), (2 0 0), and (2 1 1) planes, respectively.) were not observed either [39,40]. That is, the absence of peak variation was recognized before and after the hydrogen reduction.

Based on this literature, it is clear that the present Ru/C catalyst is neither the metal crystal nor the RuO_2 crystal of the rutile type. To sum up, the solid state of ruthenium might be an amorphous state, as the H_2-TPR profile of the catalyst (Fig. 2) is indicated strongly to be an amorphous RuO_2 state.

Although the X-ray diffractogram cannot provide conclusive evidence of the ruthenium metal plane, in the later section, we adopted the Ru_{10} model cluster with the (0 0 1) plane in order to investigate the adsorption state of the chlorobenzenes on the Ru/C catalyst, because the (0 0 1) plane is the highest atomic density in the whole plane.

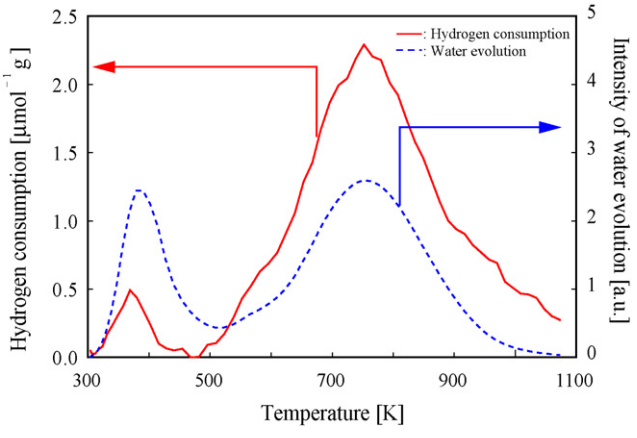

Fig. 2. Hydrogen consumption and water evolution in the temperature-programmed reduction (TPR) of the Ru/C catalyst.

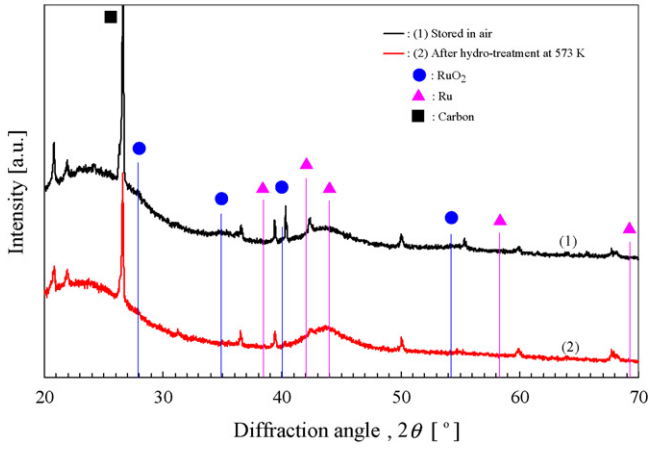

Fig. 3. X-ray diffraction pattern of the Ru/C catalyst: (1) exposure to air at room temperature and (2) after reduction in hydrogen at 573 K.

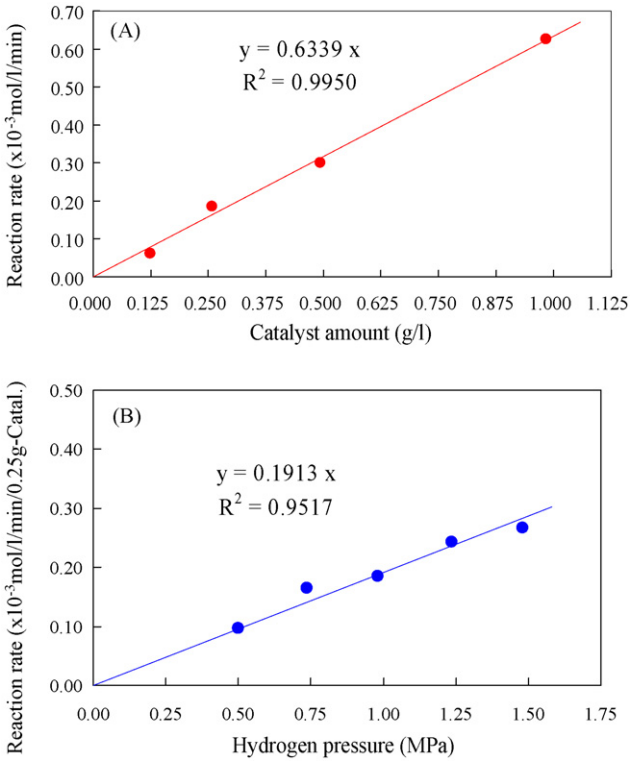

Fig. 4. Variation of the HDC reaction rate of chlorobenzene (CLB): (A) relationship between the HDC reaction rate and the catalyst amount and (B) relationship between the HDC reaction rate and the hydrogen pressure.

3.2. Hydrodechlorination

3.2.1. Mass transfer resistances

Since the present HDC of chlorobenzene and their *para*-isomers were carried out in the liquid phase using the solid catalyst Ru/C, both the mass transfer resistance and diffusion resistance are expected to directly influence the reaction rate. Therefore, the effect of the catalyst amount on the initial reaction rate was investigated using the most basic substrate of chlorobenzene (CLB) 50×10^{-3} mol/l, at 523 K. In the reaction of this model compound, benzene was produced selectively and none of the ring hydrogenated compounds (such as cyclohexene and cyclohexane) were detected.

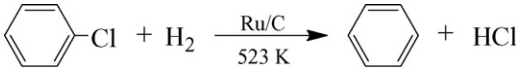

(2)

In the course of the present reaction, the absence of mass transfer resistances for the gas–liquid and the liquid–solid phases may be evidenced by three independent experiments (namely, agitation speed, catalytic amount and hydrogen pressure) [24,25]. Concerning the agitation speed, it was observed that the HDC reaction rate constants of the model reaction retain a steady value at an agitation speed of over 300 rpm. However, for the sake of completeness, all reactions were carried out at 1200 rpm. For the catalytic amount, as shown in Fig. 4A, a good linear relationship (the square of correlation coefficient (R^2 = 0.9950)) was observed within the range of 0.125–1.0 g/l. For the effect of the hydrogen pressure, furthermore, a good linear relationship (R^2 = 0.9517) was also observed within the range 0.5–1.5 MPa, which is shown in Fig. 4B. Based on these results, it is confirmed that none of the mass transfer resistances were in existence.

3.2.2. Products distribution

In order to investigate the electronic effect of the substituent of the *para*-substituted chlorobenzenes on the HDC over the Ru/C catalyst, ordinary reactions were carried out under a catalyst 0.25 g/l, hydrogen pressure 1.0 MPa, agitation speed of 1200 rpm and a reaction temperature of 523 K.

In the reaction of *para*-isomers of chloroaniline (CLAN), chloroanisole (CLAS) and chlorotoluene (CLTN) (these have the electron-donating substituent), and of dichlorobenzene (DCLB), trifluoromethylchlorobenzene (CLTF) (these have the electron-withdrawing substituent), the HDC by the reductive cleavage of carbon–chlorine bond occurred selectively and the corresponding *mono*-substituted benzenes were produced.

In the case of chloroacetophenone (CLAP) and chlorobenzonitrile (CLBN), as shown in Table 3, wide varieties of the products

Table 3
Reaction conversion and selectivity for the hydrodechlorination of chlorobenzenes[a]

Substrate	Time (min)	Product	Conversion (mol%)	Selectivity[b] (mol%)
p-Chloroaniline (CLAN)	4.5	Aniline	5	100
p-Chloroanisole (CLAS)	30	Anisole	6	100
p-Chlorotoluene (CLTN)	60	Toluene	9	100
Chlorobenzene (CLB)	36	Benzene	13	100
p-Dichlorobenzene (DCLB)	18	Chlorobenzene	2	100
p-Trifluoromethyl-chlorobenzene (CLTF)	120	Trifluoromethylbenzene	A trace	100
p-Chloroacetophenone[c] (CLAP)	60		8	
		Ethylbenzene		29
		p-Chloroethylbenzene		19
		Acetophenone		43
		4-Chloro-α-methyl-benzylalcohol		9
p-Chlorobenzonitrile (CLBN)	60		100	
		Toluene		9
		Benzonitrile		–
		Benzylamine		2
		p-Chlorobenzylamine		30
		Unknown[d]		4
		bis(4-Chlorobenzyl)amine		55

[a] Substrate (4×10^{-3} mol, except for CLAP), solvent (40 ml), and catalyst (0.01 g) were employed.
[b] Determined by GLC analysis using an internal hydrocarbon standard (toluene or *m*-xylene).
[c] Substrate amount was 2×10^{-3} mol for CLAP.
[d] No identification by GC-MS analysis.

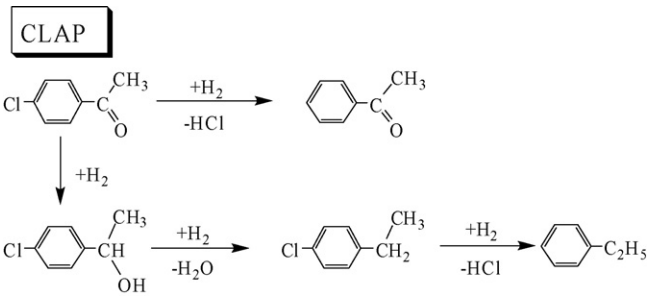

Fig. 5. HDC reaction pathway suggested for *p*-chloroacetophenone (CLAP).

were detected. Namely, in the reaction of CLAP, acetophenone, ethylbenzene and *para*-chloroethylbenzene were mainly produced, although the conversion is very low (8%) at the reaction time. This product distribution suggests that the hydrogenation and/or hydrogenolysis of the *para*-substituent (namely, acetyl functional group) occurred stepwise, accompanying the direct HDC by the reductive cleavage of the carbon–chlorine bond. The suggested reaction pathways are shown in Fig. 5. When compared with *para*-chloroethylbenzene (CLEB) as a substrate using a TOF, CLAP has slightly high reactivity in the criterion for overall conversion at 60 min (CLAP: 3.4 min^{-1}, CLEB: 3.1 min^{-1}, respectively). As for the total conversion of the HDC products, in contrast, CLAP has less HDC reactivity at 60 min (CLAP: 2.4 min^{-1}, CLEB: 3.1 min^{-1}, respectively), because of the competitive reaction caused in CLAP.

In the reaction of CLBN, on the other hand, large amounts of bis(4-chlorobenzyl)amine were detected as a characteristic product, accompanied with a considerable amount of *para*-chlorobenzylamine, whereas no benzonitrile was detected at a reaction time of 60 min. This result suggests that the hydrogenation of the cyano functional group following the condensation reaction of the intermediate such as *para*-chlorobenzylamine analogue occurred in the catalytic surface.

For CLAP and CLBN, these features of HDC reactivity were observed previously in the reaction over the Pt/C catalyst [23]. In the catalytic reduction of *para*-chloronitrobenzene, using the Ni/C, Ni/γ-Al_2O_3, Ni/SiO_2 and Raney Ni catalyst, furthermore, Wu et al. also reported that hydrogenolysis of the electron-withdrawing substituent (namely, the $-NO_2$ functional group) took place selectively and chloroaniline (CLAN) was the only product [22]. Along with the Ni and Pt catalysts, in the case of the Ru catalyst, it may be also characteristic that the π-electron-rich part of the organic reactant is attacked electrophilically by the proton (H^+) of the catalytic surface.

For the reasons mentioned above, CLAP and CLBN were excluded from the model compound of the present kinetic analysis.

3.2.3. Reaction rate constants

With respect to the concentration of each reactant, HDC reaction rates were approximately first order (0.92–0.99 orders, accurately) within the range 25×10^{-3} to 100×10^{-3} mol/l; results are shown in Fig. 6A and B.

For substituted chlorobenzenes with an electron-donating substituent, the rate constant decreased in the order of CLAN ≫ CLB ≈ CLTN ≈ CLAS (Fig. 6A). Overall, since the magnitude of the electron-donating ability is decreased in the order of $-NH_2 > -OCH_3 > -CH_3 > -H$, none of the regularity of the rate constant is observed in the above order. In the case of chlorobenzenes possessing an electron-withdrawing substituent, on the other hand, the rate constant decreased in the following order: CLB > DCLB ≫ CLTF (Fig. 6B). In contrast with the electron-donating substituent, it is clear that the HDC is prevented by the existence of the electron-withdrawing substituent.

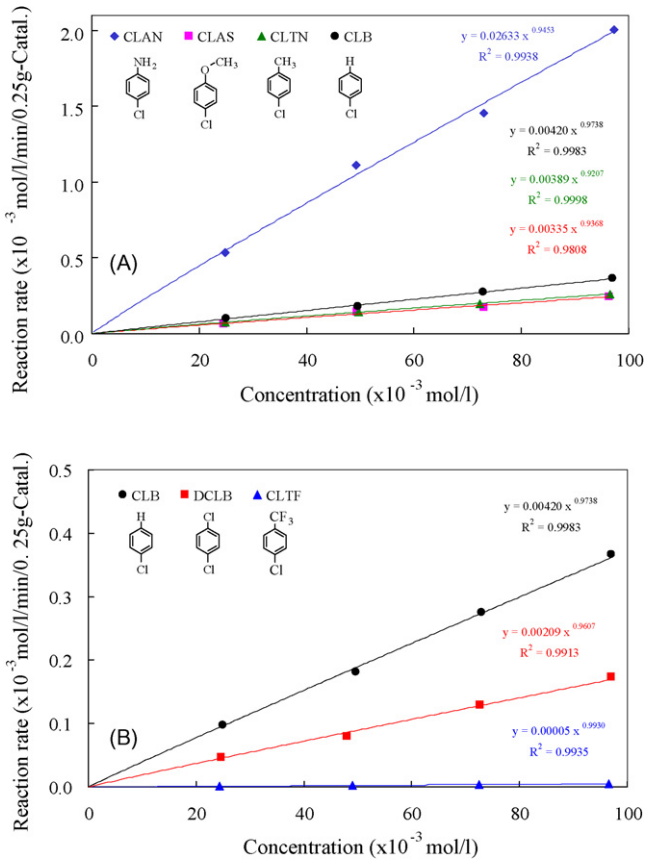

Fig. 6. Reaction rates of chlorobenzene and the *para*-isomer with substituents according to the substrate concentration: (A) electron-donating substituent and (B) electron-withdrawing substituent.

Several papers have reported the effect of the electron-donating substituent on the HDC of chlorobenzenes. In the gas phase reaction over Ni/γ-Al_2O_3, the following order of the reactivity is reported by Suzdorf et al.: *p*-NH_2 (CLAN) > *p*-OH (chlorophenol) > *p*-CH_3 (CLTN) > *p*-H (CLB) [21]. By Keane et al., a different trend was observed in the HDC of some chlorobenzenes over Ni/SiO_2 catalyst: 4-CH_3 (CLTN) > 4-OH > *p*-H (CLB) [19]. Furthermore, in the liquid phase reaction over the various Ni catalyst, Wu et al. obtained the following good linear relationship between the rate constant ratio ($\log k/k_H$) and the Hammett constant (σ_p): CLB > *p*-CH_3 (CLTN) > *p*-NH_2 (CLAN) > *p*-O^- [22]. Despite the reaction using the same catalytic element, it is surprising to note a lack of correlation between the HDC reactivity of the chlorobenzenes and the catalytic element. To compare the HDC reactivity with respect to one another, further accumulation of experimental data compiled under the same conditions may be required.

In order to examine the relevant degree of the electronic property to the HDC reactivity, the Hammett equation was applied to the above results:

$$\ln\left(\frac{k}{k_0}\right) = \rho\sigma \qquad (2)$$

where k is the HDC reaction rate constant of the substituted chlorobenzenes, k_0 the rate constant of chlorobenzene, ρ the reaction constant and σ is the Hammett's substitution constant.

For electron-donating substituents, as shown in Fig. 7, none of the methodical tendency was observed between $\ln(k/k_0)$ and σ_p^0. On the other hand, as for chlorobenzenes possessing the electron-

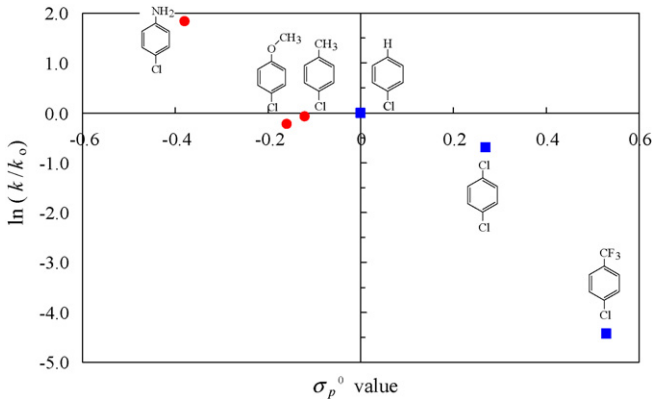

Fig. 7. Plots of the HDC reaction rate constant of the *para*-substituted chlorobenzenes to the substitution constant (σ_p^0).

withdrawing substituent, although no linear relationship between $\ln(k/k_0)$ and σ_p^0 was found, it is clear that the *para*-substituted chlorobenzene of the lager σ_p^0 value was showing to the smaller $\ln(k/k_0)$ value; that is, the HDC reactivity was depressed by the existence of the electron-withdrawing substituent.

It is suggested that the reactant of the negative reaction constant ($\rho < 0$) is π-electron rich at the reaction center (namely, the carbon atom in the C–Cl bond), meaning that an electrophilic reaction occurs. Although the present result for the electron-withdrawing substituent does not fit the linear equation, it is inferred that the electronic property showing with an σ_p^0 value affects the HDC reaction to some extent as the order of the magnitude of the σ_p^0 value is qualitatively consistent with that of the reaction constant ($\ln k/k_0$). On the other hand, from the standpoint of the directing effect of *ortho*-, *para*- and/or *meta*-substituted benzene, it is expected in general that the π-electron density on the carbon atom in the C–Cl bond is increased by the existence of the electron-donating substituent in *para*-position, whereas the density is decreased by the electron-withdrawing substituent. For the metallic surface of the catalyst, as mentioned above, it is also expected that the π-electron-rich part in the organic reactant has higher chemical affinity to the catalytic surface than that of the π-electron poor part, and thereby the adsorption of the reactant on the surface is expected to occur more easily. Therefore, since the degree of the adsorption is expressed generally by the adsorption energy, the difference in the HDC reactivity may be connected with the magnitude of the adsorption energy, depending on the difference in the degree of the electron-donating or electron-withdrawing ability of the substituent.

To elucidate the relevance of the above consideration for the HDC reactivity, a quantum calculation was attempted to search for the adsorption state of the substituted chlorobenzenes on a simple cluster model.

3.3. Quantum calculation

In order to obtain information for the adsorption state and/or adsorption energy of chlorobenzenes on the catalytic site, theoretical calculations of the "chlorobenzenes-Ru_{10}" complex were examined using the DFT method and the B3LYP/LANL2DZ system. As shown in Fig. 8, the model cluster (Ru_{10}) in the complexes is a hexagonal closed packing (hcp) structure.

3.3.1. Adsorption states in "chlorobenzene-Ru_{10}" complex

In the calculation of the initial structures of the "chlorobenzenes-Ru_{10}" complex, initially, the chlorobenzenes were arranged above the central ruthenium atom of the (0 0 1) plane at a height of 0.150 nm through the chlorine atom (named "Type-I"). In the case of CLB, as seen in Fig. 9A and B, the chlorine-ruthenium atomic distance was extended from 0.150 to 0.471 nm after the optimization. This result shows that no interaction between the CLB and Ru_{10} cluster is expected, because the ruthenium–chlorine atomic distance ($Ru_{(No.\ 5)}$–Cl) has an excessively long range at the final geometry. Furthermore, concerning the adsorption site in the

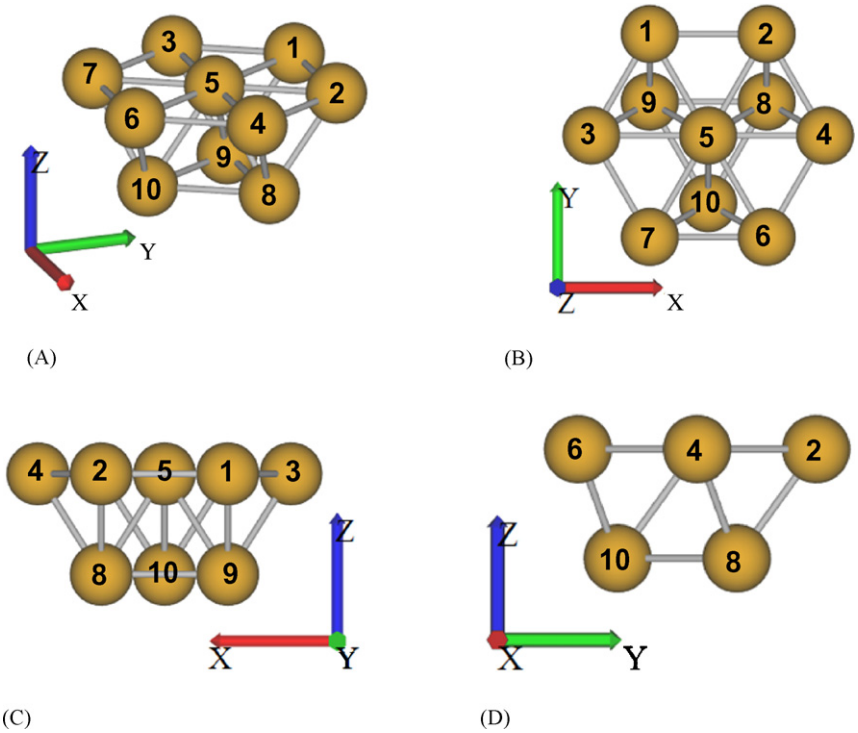

Fig. 8. The structure of Ru_{10}. (A) Bird's eye view (Ru_{10}), (B) horizontal section (*X*–*Y* plane of A), (C) vertical section (*X*–*Z* plane of A) and (d) vertical section (*Y*–*Z* plane of A)

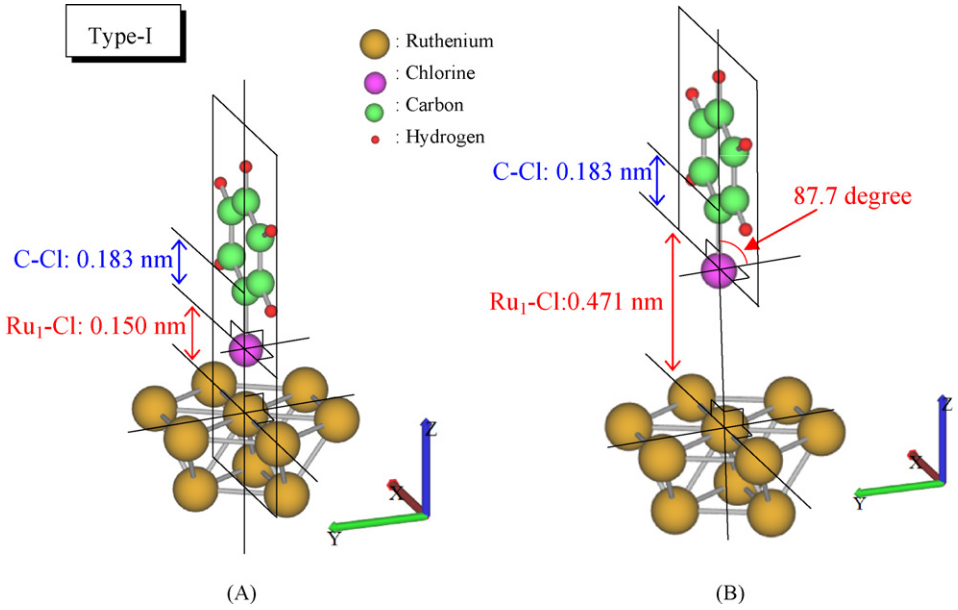

Fig. 9. (A) Initial and (B) optimized geometries for the adsorption of chlorobenzene on the center Ru atom of (0 0 1) plane in the Ru_{10} cluster ("Type-I" adsorption).

Ru_{10} cluster, it may be implied that a ridge or edge part is suitable for chlorobenzenes rather than the center of the (0 0 1) plane because the nuclear repulsion predominantly occurs between the adsorbate and the plane. A similar tendency of the final geometry to the Type-I adsorption was observed in a previous paper [23], where CLB was put on the center atom of the (0 0 1) plane of the Pt_{14} model cluster at a height of 0.200 nm.

On the other hand, when CLB was placed above a height of 0.150 nm of the midpoint of two ridge ruthenium atoms ($Ru_{(No.\ 1)}$, $Ru_{(No.\ 2)}$) through the chlorine atom at an angle of 45° of the molecular axis (named "Type-II"), a great stable point was found in the optimization (Fig. 10A and B, respectively). In this final structure, the adsorption distance from the Cl atom to the midpoint of the $Ru_{(No.\ 1)}$–$Ru_{(No.\ 2)}$ bond was lengthened from 0.150 nm to 0.269 nm (namely, $Ru_{(No.\ 1)}$–Cl, $Ru_{(No.\ 2)}$–Cl: 0.301 nm). Moreover, the carbon–chlorine atomic distance was slightly expanded from 0.183 to 0.187 nm. Except for CLAN, similar adsorption states to CLB were also observed in all the substituted chlorobenzenes. On the other hand, in the case of the optimization of CLAN, the chlorine atom falls on the lower position in the *z*-coordinate below the *x*–*y* plane of the Ru_{10} cluster, in contrast to the chlorine atom in the other chlorobenzenes, which are located in the position above the (0 0 1) plane of the Ru_{10} cluster. Actually, the final geometry in CLAN reveals that the chlorine atom slips down along with the plane surrounded by the four ruthenium atoms ($Ru_{(No.\ 1,\ No.\ 2,\ No.\ 8,\ No.\ 9)}$). Therefore, secondly, the adsorption energies were checked out for these chlorobenzenes.

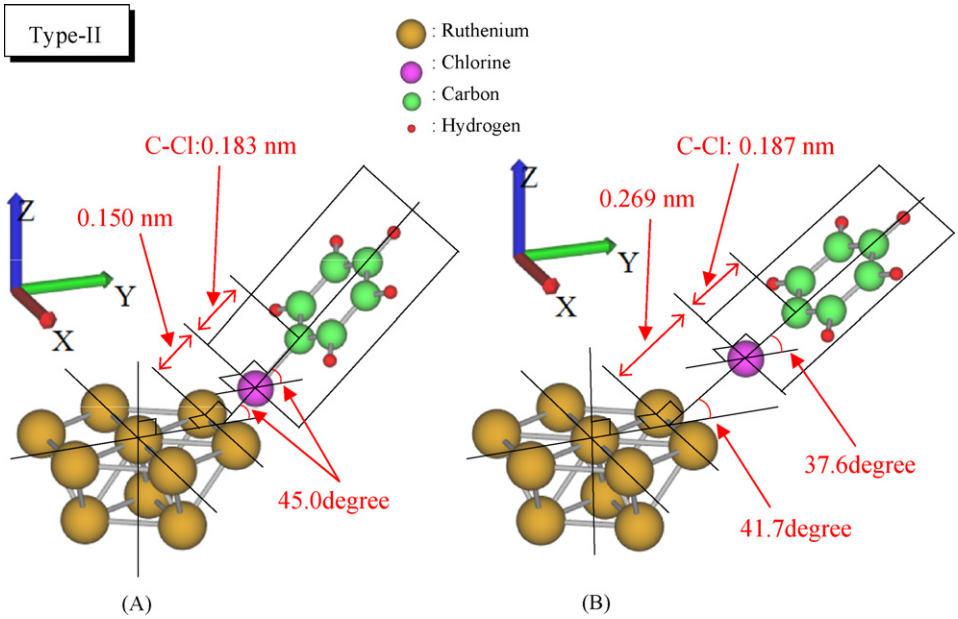

Fig. 10. (A) Initial and (B) optimized geometries for the adsorption of chlorobenzene above the midpoint of two ridge Ru atoms ($Ru_{(No.\ 1)}$–$Ru_{(No.\ 2)}$) in the Ru_{10} cluster for "Type-II" adsorption.

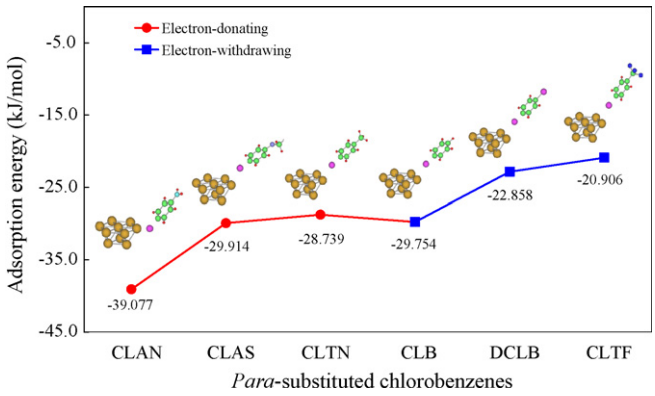

Fig. 11. Adsorption energy (E_{ad}) of chlorobenzenes on the Ru_{10} cluster for "Type-II" adsorption.

3.3.2. Adsorption energy in "chlorobenzenes-Ru_{10}" complex

In the previous study concerning the HDC of chlorobenzenes over a Pt/C catalyst [23], we reported the relationship between the order of the HDC reactivity and that of the magnitude of adsorption energy. Expecting to find a similar relationship, in the present study, the adsorption energy for the "chlorobenzenes-Ru_{10}" complex of Type-II was investigated.

The adsorption energy (E_{ad}) of the chlorobenzenes was defined as below:

$$E_{ad} = E_{complex} - (E_{chlorobenzenes} + E_{Ru_{10}\ cluster})$$

where $E_{complexes}$ is the potential energy in the optimized geometry of the "chlorobenzenes-Ru_{10}" complex, $E_{chlorobenzenes}$ the potential energy in the optimized geometry of each chlorobenzene, and $E_{Ru_{10}\ cluster}$ is the potential energy in the single point calculation of the Ru_{10} cluster, respectively.

For chlorobenzenes with an electron-donating substituent, as seen in Fig. 11 (the four circles on the left side), the magnitude of E_{ad} (absolute value) in the Type-II adsorption decreased in the order of *p*-chloroaniline (CLAN) > *p*-chloroanisole (CLAS) ≈ chlorobenzene (CLB) ≈ *p*-chlorotoluene (CLTN). This order is similar to that of the experimental one. CLAN in this series resulted in a great deal of adsorption. On the other hand, in the case of chlorobenzenes with electron-withdrawing substituent (the three squares on the right side in Fig. 11), the magnitude of E_{ad} in the Type-II adsorption decreased in the following order: chlorobenzene (CLB) > *p*-dichlorobenzene (DCLB) > *p*-trifluoromethylchlorobenzene (CLTF), while the order of the E_{ad} was in positive agreement with that of the actual HDC reactivity.

Since the larger adsorption energy in CLAN than the other chlorobenzenes is indicative of the larger interaction between the CLAN and Ru_{10} cluster, both the interacting orbital and the energy level in all the chlorobenzenes were checked and shown in Figs. 12 and 13. In the orbital interaction of CLAN, as seen in Fig. 12A, HOMO-2 (−0.292 eV) of CLAN interacted with the doubly degenerated LUMO + 1 (−0.118 eV) and produced two orbitals both of HOMO-42 (−0.329 eV) and LUMO + 7 (−0.087 eV). In the case of other chlorobenzenes, such as CLAS and CLB, HOMO-2 or HOMO-3 of the chlorobenzenes interacted with both the doubly degenerated LUMO + 3 (−0.114 eV) and the doubly degenerated HOMO-25 (−0.321 eV), and produced the two orbitals of the more stable occupied orbital and the more unstable unoccupied orbital. As a representative result, the orbital interaction for CLB is shown in Fig. 12B. As seen in Fig. 13A and B, furthermore, the HOMO-2 on the chlorine atom in CLAN is a p_z-type orbital when the benzene ring is put in the *x*–*y* plane, while the interacting orbital in other chlorobenzenes is the p_y-type orbital in every case. In addition, all of these orbitals have an anti-node of the C–Cl bond, which is advantageous to the bond scission, following the adsorption of chlorobenzenes on the catalytic surface. Also, the energy level of HOMO-2 in CLAN is suggestive of the higher HDC reactivity of CLAN. As shown in Fig. 13C, the energy level of the interacting molecular orbital in the chlorobenzenes is decreased in the order of CLAN (−0.292 eV) < CLAS (−0.311 eV) ≈ CLTN (−0.311 eV) < CLB (−0.314 eV); CLB < DCLB (−0.323 eV) < CLTF (−0.335 eV). Since the smaller energy gap between two interacting orbitals generates the larger orbital interaction, it is expected that the orders of the reactivity of the chlorobenzenes are decreased in the inverse order with the height of the energy level: CLAN > CLAS > CLTN > CLB; CLB > DCLB > CLTF, respectively. This order is also similar to that of the experimental HDC reactivity. To conclude, for the reason of the highest HDC reactivity of CLAN, it is suggested that the highest energy level of HOMO-2 of CLAN in connection with the characteristic orbital shape is important for interaction with the lower catalytic orbital of LUMO + 1.

As a role of the solid catalyst, the activation energy is diminished by the existence of the catalyst, alongside the increase in the collision number on the surface. For the reason of this diminishing effect of the activation energy, the adsorption of the reactant on the catalytic site is a significant factor in the first step of the reaction. When a catalyst is used in the reaction of homolog's reactants, therefore, it is expected in general that the larger adsorption energy of an adsorbate gives smaller activation energy, thus facilitating the reaction. In the present study, the fact that the sequence of the adsorption energy is in close agreement with that of the actual HDC reactivity may be suggestive of the availability of the adsorption energy as the reactivity index of the HDC reactivity.

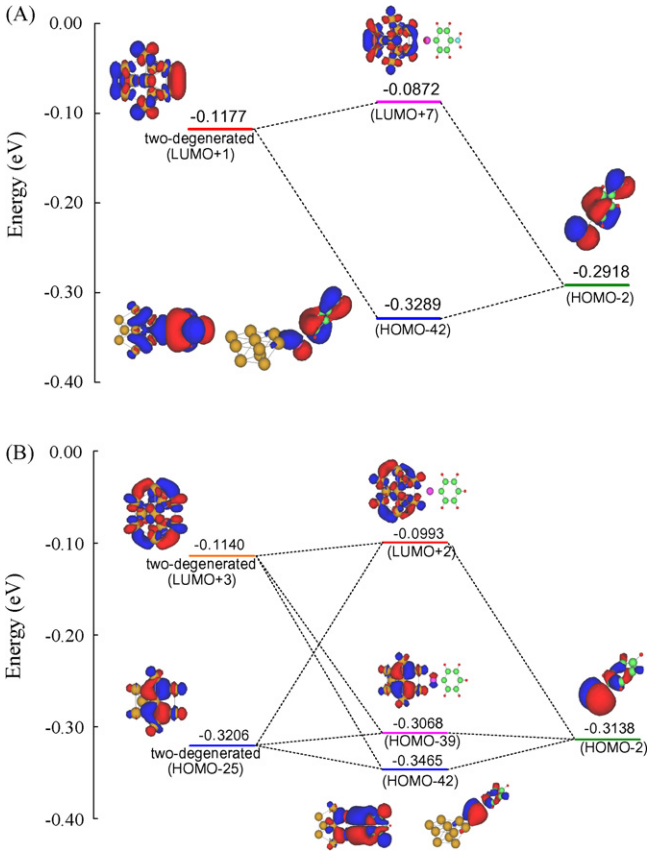

Fig. 12. Difference of the orbital interaction between the chlorobenzenes and the Ru_{10} cluster: (A) CLAN and (B) CLB.

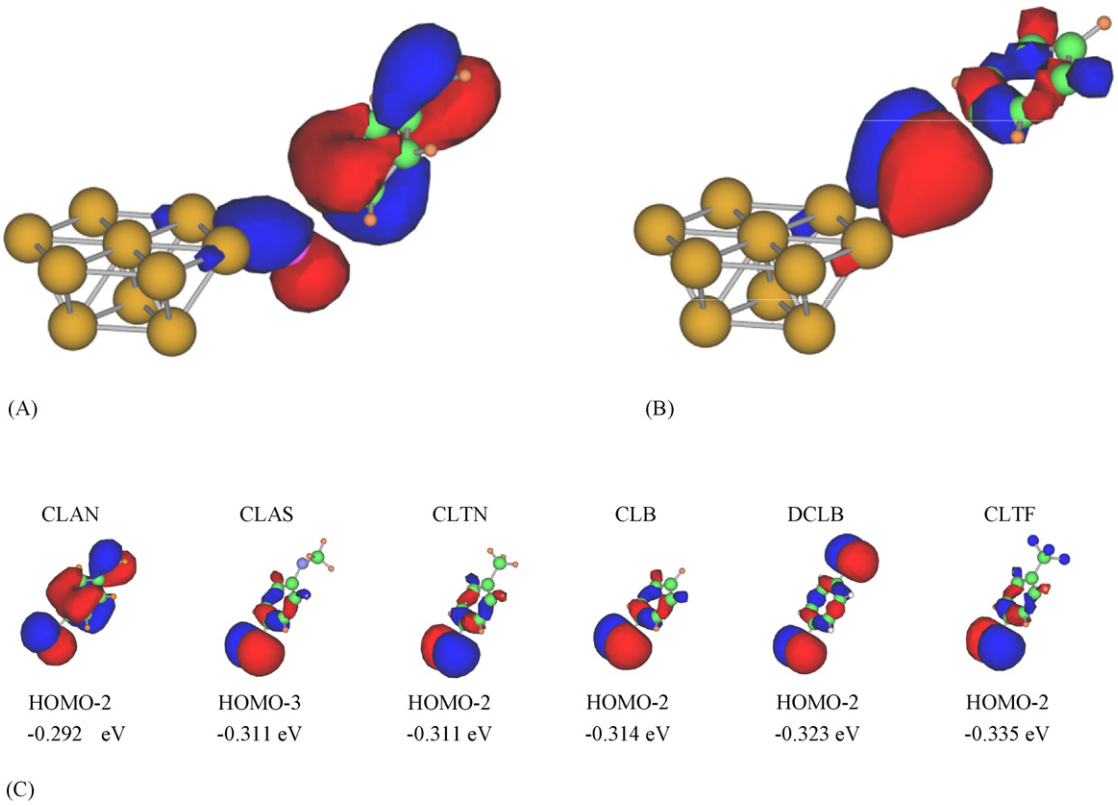

Fig. 13. Interacting orbital of (A) "CLAN-Ru_{10}" complex, (B) "CLB-Ru_{10}" complex and (C) chlorobenzenes.

However, two subjects remain. The first subject is exploration of a suitable adsorption site where the dissociative adsorption of chlorobenzenes through the carbon and chlorine atoms of the C–Cl bond occurs. As a practical matter, in the kinetic study, Serguchev reported the formation of the σ-complex by dissociative adsorption [28]. The second subject, in relation to exploration of a suitable cluster model, is to clarify the structure of the Ru/C catalyst under the present reaction condition, which was assumed to be an amorphous state based on the standpoint of the XRD analysis. A more comprehensive XRD study on the catalyst may be needed alongside other analytical methods, e.g. XPS, TEM, and so forth.

4. Conclusion

(1) Using the 5%-Ru/C catalyst, the hydrodechlorination (HDC) reactivity of chlorobenzene and *para*-substituted chlorobenzenes with the electron-donating and electron-withdrawing substituent was examined. In addition, the catalytic characterization of the Ru/C was checked from the standpoint of the textural properties, decomposition of the functional group on the carbon surface (TPD), H_2 consumption (TPR) and XRD analyses.

(2) In the hydrodechlorination (HDC) of chlorobenzene (CLB) and *para*-amino, -methoxy, -methyl, -chloro and -trifluoromethyl substituted chlorobenzenes (abbreviated as CLAN, CLAS, CLTN, DCLB and CLTF, respectively), the reductive cleavage of the carbon–chlorine (C_{sp_2}–Cl) bond proceeded selectively. In the reaction of *para*-cyano and -acetyl substituted chlorobenzenes, on the other hand, the hydrogenation and/or hydrogenolysis of the substituent took place preferentially.

(3) When the HDC rate constants were compared with respect to one another, the HDC reactivity of chlorobenzenes with electron-donating and electron-withdrawing substituent decreased in the orders of CLAN $\gg$ CLB $\approx$ CLTN $\approx$ CLAS and CLB > DCLB $\gg$ CLTF, respectively. Correlation between the rate constants and the Hammett substitution values (σ_p^0), although these reactivities of chlorobenzenes did not reveal a proportional regularity according to the ability of the electron-donating and the electron-withdrawing substituent, the HDC reactivity was depressed in good order with the existence of the electron-withdrawing equivalent.

(4) In the geometry optimization using the DFT method (B3LYP/LANL2DZ), when chlorobenzenes were placed above a height of 0.150 nm of the midpoint of two ridge ruthenium atoms ($Ru_{(No.\ 1)}$, $Ru_{(No.\ 2)}$) through the chlorine atom at a molecular axis angle of 45° (named "Type-II"), a considerable stable point was found. The magnitude of the adsorption energy decreased in the order of CLAN > CLAS $\approx$ CLB $\approx$ CLTN and CLB > DCLB > CLTF, respectively. Since these orders were similar to that of HDC reactivity, it was concluded that the adsorption energy may be useful for the HDC reactivity index.

(5) From the inspection of the orbital interactions, for the evolution of the largest adsorption energy in CLAN, it was suggested that both the highest energy level and the characteristic orbital shape of the interacting orbital (HOMO-2: $E = -0.292$ eV) is important.

Acknowledgement

We would like to thank Dr. Koshiro Koizumi for his experimental assistant with the X-ray diffraction analysis.

References

[1] W.J. Stry, J.D. Felske, N. Ashgriz, Environ. Eng. Sci. 20 (2003) 125–133.
[2] K.S. Kim, K.H. Hong, Y.H. Ko, J. Air Waste Manage. Assoc. 54 (2004) 555–562.
[3] G. Rouzet, D. Schwartz, R. Gadiou, L. Delfosse, J. Anal. Appl. Pyrolysis 57 (2001) 153–168.

[4] O. Kranz, J. Voss, Chem. Sci. 58 (2003) 1187–1200.
[5] H. Cheng, K. Scott, P.A. Christensen, J. Electroanal. Chem. 566 (2004) 131–138.
[6] H. Yin, Y. Wada, T. Kitamura, S. Yanagida, Environ. Sci. Technol. 35 (2001) 227–231.
[7] A. Tiehm, I. Kohnagel, U. Neis, Water Sci. Technol., 1st World Congress, Part 2: Industrial Wastewater and Environmental Contaminants, vol. 43, no. 2, 2000, pp. 297–303.
[8] J.G. Rodoríguez, A. Lafuente, Tetrahedron Lett. 43 (2002) 9645–9647.
[9] P.J.M. Middeldorp, W.V. Doesburg, G. Schraa, A.J.M. Stams, Biodegradation 16 (2005) 283–290.
[10] U.R. Pillai, E. Sahle-Demessie, R.S. Varma, Green Chem. 6 (2004) 295–298.
[11] B.F. Hagh, D.T. Allen, in: H.M. Freeman (Ed.), Innovative Hazardous Waste Treatment Technology, vol. 1, Technomic, Lancaster, PA, 1990, pp. 45–53.
[12] W. Wu, J. Xu, Catal. Commun. 5 (2004) 591–595.
[13] S.S. Zinovyev, N.A. Shinkova, A. Perosa, P. Tundo, Appl. Catal. B: Environ. 55 (2005) 39–48.
[14] J.L. Benitez, G.D. Angel, React. Kinet. Catal. Lett. 70 (2000) 67–72.
[15] L.M. Gómez-Sainero, A. Cortés, X.L. Seoane, A. Arcoya, Ing. Eng. Chem. Res. 39 (2000) 2849–2854.
[16] B.C. Beard, Z.C. Zhang, Catal. Lett. 82 (2002) 1–5.
[17] M.A. Keane, P.M. Patterson, Catal. Lett. 99 (2005) 33–39.
[18] Y. Hashimoto, Y. Uemichi, A. Ayame, Appl. Catal. A: Gen. 287 (2005) 89–97.
[19] M.A. Keane, Appl. Catal. A: Gen. 271 (2004) 109–118.
[20] K. Konuma, N. Kameda, J. Mol. Catal. A: Chem. 178 (2002) 239–251.
[21] A.R. Suzdorf, S.V. Morozov, N.N. Anshifts, S.I. Tsiganova, A.G. Anshifts, Catal. Lett. 29 (1994) 49–55.
[22] W. Wu, J. Xu, R. Ohnishi, Appl. Catal. B: Environ. 60 (2005) 129–137.
[23] T. Yoneda, T. Takido, K. Konuma, J. Mol. Catal. A: Chem. 265 (2007) 80–89.
[24] V. Felis, C.D. Bellefon, P. Fouiloux, D. Schweich, Appl. Catal. B: Environ. 20 (1999) 91–100.
[25] P.D. Vaidya, V.V. Mahajani, Appl. Catal. B: Environ. 51 (2004) 21–31.
[26] A.C.B. Silva, A.P.G. De Sousa, J.D. Ardisson, H.G.L. Siebald, E. Moura, E.N. Dos Santos, N.D.S. Mohallem, R.M. Lago, Mater. Res. 6 (2003) 137–144.
[27] A. Malinowski, W. Juszcyk, J. Pielaszek, M. Bonarowska, M. Wojciechowska, Z. Karpiński, Chem. Commun. 8 (1999) 685–686.
[28] Yu.A. Serguchev, Yu.V. Belokpytov, Kinet. Catal. 42 (2001) 195.
[29] H.E. Swanson, R.K. Fuyat, G.M. Ugrinic, NBS Circular 539 4 (1955) 5–6.
[30] Æ. Frisch, M.J. Frisch, G.W. Trucks, Gaussian03 User's Reference, Gaussian Inc., Pittsburgh, PA, 2003, pp. 73–78.
[31] A.D. Becke, J. Chem. Phys. 98 (1993) 5648–5652.
[32] C. Lee, W. yang, R.G. Parr, Phys. Rev. B 37 (1988) 785–789.
[33] P.J. Hay, W.R. Wadt, J. Chem. Phys. 82 (1985) 270–283.
[34] C. Park, M.A. Keane, J. Catal. 221 (2004) 386–399.
[35] M.C.R. Martínez, D.C. Amarós, A.L. Solano, C.S.M. De Lecea, Carbon 31 (1993) 895–902.
[36] S.Y. Haung, S.M. Chang, C.T. Yeh, J. Phys. Chem. B 110 (2006) 234–239.
[37] T.L. Stuchinskaya, M. Musawir, E.F. Kozhevnikova, I.V. Kozhevnikov, J. Catal. 231 (2005) 41–47.
[38] S.F. Yin, B.Q. Xu, W.X. Zhu, C.F. Ng, X.P. Zhou, C.T. Au, Catal. Today 93–95 (2004) 27–38.
[39] V.I. Zailkovskii, K.S. Nagabhushana, V. Kriventov, K.N. Loponov, S.V. Cherepanova, R.I. Kvon, H. Bönnemann, D.I. Kochubey, E.R. Savinova, J. Phys. Chem. B 110 (2006) 6881–6890.
[40] M.C. Santos, . Cogo, S.T. Tanimoto, M.L. Calegaro, L.O.S. Bulhões, Apple. Surf. Sci. 253 (2006) 1817–1822.